

LM-07K003
April 5, 2007

Raman Spectroscopy Determination of Hole Concentration in p-Type GaSb

JE Maslar, WS Hurst, CA Wang

NOTICE

This report was prepared as an account of work sponsored by the United States Government. Neither the United States, nor the United States Department of Energy, nor any of their employees, nor any of their contractors, subcontractors, or their employees, makes any warranty, express or implied, or assumes any legal liability or responsibility for the accuracy, completeness or usefulness of any information, apparatus, product or process disclosed, or represents that its use would not infringe privately owned rights.

Raman Spectroscopic Determination of Hole Concentration in p-Type GaSb

J. E. Maslar^{a)} and W. S. Hurst

Chemical Science and Technology Laboratory, National Institute of Standards and Technology
100 Bureau Drive, Stop 8360, Gaithersburg, MD 20899-8360

C. A. Wang

Lincoln Laboratory, Massachusetts Institute of Technology
244 Wood Street, Lexington, MA 02420-9108

Room temperature p-type GaSb bulk coupled mode spectra were measured as a function of hole concentration. These spectra were obtained using an optical system based on 752.55 nm excitation in order to obtain more sensitivity to bulk GaSb coupled mode scattering than possible with visible wavelength excitation-based systems. A relatively simple spectral model for the electronic contribution to the dielectric function was evaluated for determination of hole concentration from the bulk coupled mode spectra. Optically-derived values for hole concentration were determined by minimizing the sum of the residuals squared between an experimental and simulated spectrum as a function of total hole concentration and a plasmon damping parameter. Hole concentrations obtained from the Raman spectroscopic measurements deviated from the values determined from single field Hall effect measurements that were corrected to account for two band conduction by $\approx 20\%$ to $\approx 65\%$. These deviations were attributed to the limitations of the spectral model employed and uncertainties in GaSb materials properties.

Keywords: accumulation layer; gallium antimonide; GaSb; hole concentration; p-type doping; Raman spectroscopy

^{a)}Author to whom correspondence should be addressed; electronic mail: jmaslar@nist.gov

The Lincoln Laboratory portion of this work was sponsored by the Department of Energy (DOE), under Air Force contact number FA8721-05-C-0002. The opinions, interpretations, conclusions and recommendations are those of the authors and are not necessarily endorsed by the United States Government.

INTRODUCTION

GaSb and related alloy semiconductors, e.g., GaInAsSb and GaInSb, are of interest for mid-infrared sources and detectors and low-power, high-speed electronic devices.¹⁻³ Carrier transport is central to the operation of all such devices and measurement of carrier concentration and mobility is critical in determining the material quality and predicting device operational parameters. Single magnetic field Hall effect measurements are widely used to determine carrier concentration and mobility in semiconductors. However, a requirement for unambiguous interpretation of single magnetic field Hall measurements is the presence of only one carrier type.⁴ To avoid interference from substrate conduction in single magnetic field Hall effect measurements, epitaxial films are typically grown on semi-insulating (SI) substrates. However, SI GaSb substrates are not readily available. Therefore, epitaxial GaSb (and related materials) is often grown on SI GaAs for transport property characterization. While useful information can be obtained from GaSb epilayers grown on SI GaAs, it has been shown that the degree of dopant incorporation in GaSb epilayers grown on GaAs and GaSb substrates under nominally identical conditions can be different.⁵ Capacitance-voltage measurements can be used to obtain carrier properties on epilayers grown on a conducting substrate. However, this technique requires an electrical contact, as do Hall effect measurements. This requirement precludes the use of either technique *in situ* during growth or processing. As an optical technique, Raman spectroscopy does not suffer from these limitations. In addition, this technique is non-destructive and spatially-resolved on micron length scales.

Raman spectroscopy has been widely employed to investigate carrier properties in numerous compound semiconductor materials via observation of so-called coupled phonon-

plasmon modes, resulting from interaction between the polar longitudinal optic (LO) phonon mode and the collective carrier plasmon mode.⁶ Numerous investigations of coupled mode Raman spectra in n-type doped III-V materials have been reported and the dependence of coupled mode spectra on electron concentration is reasonably well understood for a number of materials.⁶⁻⁹ Fewer investigations of coupled mode spectra in p-type doped binary III-V materials have been reported and, consequently, the dependence of coupled mode spectra on hole concentration is not as well understood for a variety of materials.

Most reported Raman spectroscopic investigations of the coupled modes in p-type III-V materials have involved GaAs.¹⁰⁻²³ In contrast, only a few investigations of p-type GaSb have been reported.²⁴⁻²⁸ Of these reports, one involves the same epilayers investigated here: zinc-doped in the range of $1.92 \times 10^{17} \text{ cm}^{-3}$ to $6.38 \times 10^{18} \text{ cm}^{-3}$, as determined from single magnetic field Hall effect measurements.²⁸ The focus of Ref. 28 was on the effects of different scattering excitation wavelengths on the observed GaSb spectra and not specifically bulk coupled mode spectra, although such spectra were shown. The report by Chen et al.²⁴ involves epilayers that were heavily carbon-doped at levels greater than 10^{19} cm^{-3} , as determined from single magnetic field Hall effect measurements. The measurements in Ref. 24 were carried out at low temperature and with 488 nm excitation and focused on dopant local vibrational mode scattering. The other three reports²⁵⁻²⁷ were apparently results from related investigations and involved only two intentionally doped bulk crystals: one doped at $\approx 4 \times 10^{18} \text{ cm}^{-3}$ and one at $\approx 4 \times 10^{19} \text{ cm}^{-3}$ (dopant identity and hole concentration measurements are not described).^{25,27} The focus of these three reports was on accumulation layer optical processes (although some bulk coupled mode scattering was described) and measurements were performed at low temperature and using visible wavelength excitation (between $\approx 457 \text{ nm}$ and $\approx 590 \text{ nm}$). None of these previous reports

attempted to extract bulk carrier concentration from the coupled mode spectra. To the authors' knowledge, no investigations concerning quantitative determination of carrier concentration in p-type GaSb using Raman spectroscopy have been reported.

In this investigation, room temperature p-GaSb bulk coupled mode spectra were measured as a function of hole concentration. These spectra were obtained using an optical system based on 752.55 nm excitation. This optical system is more sensitive to bulk GaSb coupled mode scattering than the visible wavelength excitation-based optical systems utilized in previous reports of p-GaSb Raman spectra.²⁸ A relatively simple model for quantitative determination of hole concentration from the bulk coupled mode spectra was evaluated. A simple spectral model was utilized so as to minimize model parameters and thereby limit errors associated with uncertainty in GaSb material properties. Optically-derived values for hole concentration were determined by minimizing the sum of the residuals squared between an experimental and a simulated spectrum as a function of total hole concentration and plasmon damping parameter. The hole concentrations obtained from the Raman spectroscopic measurements were compared to those obtained from single field Hall effect measurements.

II. EXPERIMENTAL PROCEDURE

A. Materials

Five p-type GaSb epilayers were investigated for this report. All epilayers were grown on SI GaAs substrates in a vertical flow, rotating-disk organometallic vapor phase epitaxy reactor using triethylgallium and trimethylantimony, as previously described.^{29,30} One epilayer was not intentionally doped but was unintentionally doped (uid) lightly p-type due to the presence of residual acceptor states, as is generally the case with nominally undoped GaSb epilayers.³ The four other epilayers were intentionally p-type doped at different concentrations

using dimethylzinc (DMZn) introduced into the growth reactor at mole fractions of 1×10^{-6} , 2×10^{-6} , 4×10^{-6} , and 10×10^{-6} . The most heavily doped epilayer (10×10^{-6} mole fraction DMZn) was grown on (001) GaAs misoriented 2° toward (100). All other epilayers were grown on (001) GaAs misoriented 6° toward $(1\bar{1}1)B$. The uid-GaSb epilayer was nominally $2.5 \mu\text{m}$ thick and deposited directly on the GaAs substrate. The most heavily doped epilayer was nominally $3.0 \mu\text{m}$ thick and was deposited on a $0.1 \mu\text{m}$ thick uid-GaSb buffer layer that was deposited on the substrate. All other epilayers were nominally $1.9 \mu\text{m}$ thick and were deposited directly on the substrate.

B. Electrical Measurements

Hole concentration and mobility were determined using single magnetic field (10 KG) Hall effect measurements based on the van der Pauw method and performed at room temperature.

C. Raman Spectroscopic Measurements

All Raman spectroscopic measurements were performed at (nominally) room temperature in a backscattering geometry described by $z(x, y)\bar{z}$, where x , y , z , and \bar{z} denote $[100]$, $[010]$, $[001]$, and $[00\bar{1}]$, respectively. Unless otherwise noted, spectra were obtained using 752.55 nm radiation from a krypton ion laser, as described previously.²⁸ Laser radiation was focused on to the specimen with a cylindrical lens and the corresponding power density at the sample was less than $\approx 9 \text{ W/cm}^2$. The power density was kept relatively low so as to minimize the effects on the spectra of laser-induced heating of the sample and minimize the generation of photoexcited carriers. Spectra obtained with the specified power density were determined to be nominally identical to those obtained with one half the power at the sample, indicating that no sample heating was occurring (within the limit of the instrumental bandpass). Collected radiation was

coupled into a single grating, 0.46 m focal length, $f/5.3$ imaging spectrograph equipped with a thermo-electrically cooled (to $-90\text{ }^{\circ}\text{C}$), 1024×256 pixel array ($26\text{ }\mu\text{m} \times 26\text{ }\mu\text{m}$ square pixels), deep depletion back-illuminated charge coupled device (BI CCD) camera system. The instrumental bandpass (FWHM) was $\approx 1.6\text{ cm}^{-1}$, unless otherwise noted. When noted, spectra were also obtained using 488 nm excitation from an argon ion laser, as previously described.²⁸ The laser power density at the sample with 488 nm excitation was less than $\approx 5\text{ W/cm}^2$. A thermo-electrically cooled (to $-90\text{ }^{\circ}\text{C}$), 1340×400 pixel array ($20\text{ }\mu\text{m} \times 20\text{ }\mu\text{m}$ square pixels), BI CCD camera system was employed and the instrumental bandpass for 488 nm excitation was $\approx 3.0\text{ cm}^{-1}$. All spectra shown represent the average of two spectra, each of which was obtained with a 300 s integration time. For 752.55 nm excitation, atomic lines from a uranium hollow cathode tube were used for wavelength calibration. For 488 nm excitation, atomic lines from an argon pen lamp were used for spectrograph wavelength calibration. All Raman scattering intensities were corrected for the wavelength-dependent response of the optical system using a white-light source of known relative irradiance, as previously described.²⁸

III. RESULTS AND DISCUSSION

A. Electrical measurements

Hall effect measurements of the hole concentration were used for comparison to the hole concentrations obtained from Raman spectroscopic measurements. To obtain a more accurate value for total hole concentration, the single magnetic field Hall effect measurements were analyzed using a two valence band model. If such a model is not used, single magnetic field Hall effect measurements provide only a weighted average of the concentration and mobility of the light and heavy holes.^{4,31,32} A critical component of the two valence band model is the calculation of the separate heavy and light hole concentrations. In this work, parabolic heavy

hole and light hole valence bands were assumed. The assumption of parabolic valence bands in the calculation of n_{corr} is obviously an oversimplification. This assumption was made because other methods for determining respective band shape and density of states were expected to produce results of unknown accuracy. The underlying reason for this expectation is the conduction band structure of GaSb compared to, e.g., GaAs. In GaSb, a small energy difference exists between the two lowest-energy conduction band minima and the higher-energy of these two minima possesses a higher density of states.³³ Hence, the higher-energy minimum is more populated at doping levels and temperatures of technical importance and is likely to influence the valence band structure more in GaSb than in, e.g., GaAs.³⁴ Methods that are expected to provide more accurate calculation of hole concentrations in, for example, GaAs typically assume only one conduction band. Examples of such methods include models in which density of states modifications due to many-body effects and high dopant concentrations are calculated using Klauder approximations³⁵ and models in which a band nonparabolicity factor is calculated using a Kane three level $\mathbf{k}\cdot\mathbf{p}$ model for the zone center band structure.^{36,37} Because of the uncertainties in the effects of additional conduction bands on the valence band structure in GaSb, it was determined to be impossible, within the scope of this work, to evaluate the relative accuracy of different models to calculate hole concentrations. Hence, a parabolic structure was assumed for these calculations.

The following expression was employed to estimate the corresponding light hole and heavy hole concentrations from the single magnetic field Hall effect measurements, assuming low magnetic field strength.³²

$$n_{Hall} = \frac{\left[n_{lh} + n_{hh} \left(\frac{\mu_{hh}}{\mu_{lh}} \right) \right]^2}{F(K_{lh})r_{lh}n_{lh} + F(K_{hh})r_{hh}n_{hh} \left(\frac{\mu_{hh}}{\mu_{lh}} \right)^2} \quad (1)$$

where n_i is the hole concentration in the respective valence band (lh = light hole and hh = heavy hole), μ_i is the hole mobility in the respective valence band, $F(K_i)$ is the shape factor of the respective valence band, K_i is the anisotropy factor for the respective valence band, and r_i is the Hall scattering factor for holes in the respective valence band. The shape factor was calculated using the expression:³²

$$F(K_i) = \frac{3K_i(K_i + 2)}{(2K_i + 1)^2} \quad (2)$$

Hole concentrations in the respective valence bands, n_i , were calculated assuming parabolic light hole and heavy hole valence bands.³⁶

$$n_i = 2 \left(\frac{2\pi k_B T m_i}{h^2} \right)^{3/2} F_{1/2}(\xi) \quad (3)$$

where k_B is the Boltzmann constant, T is the thermodynamic temperature, m_i are the respective hole effective masses, h is the Planck constant, $F_{1/2}(\xi)$ is the Fermi-Dirac integral of $1/2$ order, and ξ is the reduced Fermi energy given by

$$\xi = (E_v - E_F)/k_B T \quad (4)$$

where E_v is the energy at the top of the valence band (defined as zero) and E_F is the Fermi level. The Fermi-Dirac integral was approximated using the expressions of Van Halen and Pulfrey.^{38,39} For a given n_{Hall} , the corresponding total hole concentration as corrected for two-band conduction, n_{corr} , is then given by

$$n_{corr} = n_{lh} + n_{hh} \quad (5)$$

The parameter values used in the correction of the single field Hall effect measurement results to account for two-band conduction are listed in Table I. The DMZn mole fraction in the reactor during deposition of the epilayers investigated in this work and the corresponding single magnetic field Hall effect measurement hole concentration, n_{Hall} , and mobility, μ_{Hall} , and corrected hole concentration, n_{corr} , are listed in Table II.

B. Raman spectroscopic measurements

1. p-Type GaSb Raman Spectra

GaSb doped p-type exhibits a hole accumulation layer^{25-27,42} and a three-layer model is often used to describe this system.^{43,44} Moving from a point in the interior of the layer towards the surface, the three regions correspond to the bulk with a given hole concentration, a region between the surface and the bulk that is enriched in hole concentration relative to the bulk, and a surface region of zero hole concentration. In this three layer model and employing scattering excitation of sufficient optical penetration depth to probe the bulk, LO phonon-hole plasmon coupled mode scattering originates from both the bulk and the hole-enriched region and LO phonon mode scattering originates from the hole-depleted near-surface region. For simplicity and since the emphasis of this report is on the bulk coupled mode spectra, accumulation layer will refer to both the hole-enriched region and the hole-depleted near-surface region in subsequent discussion.

The qualitative relationship between coupled mode spectral characteristics and hole concentration can be deduced from the few reported Raman spectroscopic investigations of p-type GaSb and by analogy to p-type GaAs. The observed linewidth and peak wavenumber of the coupled mode originating in the accumulation layer are very similar to those of the LO phonon mode at low hole concentrations. As the hole concentration increases, the accumulation

layer coupled mode linewidth broadens and peak wavenumber decreases with respect to those of the LO phonon mode.²⁵⁻²⁸ Briefly summarizing the trends observed for the coupled modes originating in the bulk of p-type GaAs^{11,15,21,23} and GaSb,^{24,28} at low hole concentrations, one coupled mode is observed with a linewidth and peak wavenumber that are very similar to those of the LO phonon mode. As the hole concentration increases, the bulk coupled mode linewidth broadens with respect to that of the LO phonon mode. Also as the hole concentration increases, the bulk coupled mode peak wavenumber first increases from nearly that of the LO phonon mode (but by no more than $\approx 2 \text{ cm}^{-1}$) and then starts to decrease and approaches the TO phonon wavenumber. At higher hole concentrations, two coupled modes may be observed.^{21,28}

Figures 1 and 2 show the Raman spectra of the intentionally doped p-type GaSb epilayers compared to the uid-GaSb spectrum. In the spectra in Fig. 1, the spectral region of the most intense features is shown and the intensity of the most intense feature is normalized to unity in each spectrum to facilitate comparison of these features. In the spectra in Fig. 2, a higher wavenumber spectral region is shown (instrumental bandpass $\approx 2.9 \text{ cm}^{-1}$) and the intensity was not normalized so as to permit comparison of weaker features. In the uid-GaSb spectrum, the most intense feature is the first order LO phonon mode at $\approx 236 \text{ cm}^{-1}$ (see Fig. 1).^{45,46} As an aid to the eye, the uid-GaSb LO phonon mode wavenumber is nominally indicated by the vertical line in both figures at 235.9 cm^{-1} (ignoring the implications of the spectral bandpass on the number of significant figures in the peak wavenumber). Also observed in the uid-GaSb spectrum is the (weak) transverse optic (TO) phonon mode at $\approx 226 \text{ cm}^{-1}$ (see Fig. 1)⁴⁷ and (weak) second order combinational scattering features in the $\approx 265 \text{ cm}^{-1}$ to 276 cm^{-1} range and at $\approx 440 \text{ cm}^{-1}$ (see Fig. 2).^{47,48} The TO mode is nominally forbidden in backscattering geometry from the (100) direction and the observation of this mode is attributed to slight deviation of the

epilayer from the (100) direction.⁴⁹ It is apparent that the spectra of the intentionally doped epilayers differ significantly with respect to the uid-GaSb spectrum. Since the features observed in the uid-GaSb spectrum are attributed to pure phonon modes, the differences between the uid-GaSb and doped GaSb spectra are attributed to observation of scattering by coupled LO phonon-hole-plasmon modes.

In the spectra of the $n_{\text{corr}} = 3.45 \times 10^{17} \text{ cm}^{-3}$, $9.89 \times 10^{17} \text{ cm}^{-3}$, and $2.05 \times 10^{18} \text{ cm}^{-3}$ epilayers, the most intense feature is observed in the $\approx 237 \text{ cm}^{-1}$ to $\approx 239 \text{ cm}^{-1}$ range (near that of the LO phonon mode in the uid-GaSb spectrum) while a weak feature is observed at 226 cm^{-1} . The 226 cm^{-1} feature in these three spectra is nominally identical to that in the uid-GaSb spectrum and, therefore, is attributed to the TO phonon mode. The wavenumber of the relatively intense feature shifts from the uid-GaSb LO phonon mode wavenumber to higher wavenumber with increasing hole concentration in these spectra. These trends are consistent with those observed in Raman spectra of p-type GaAs at moderate doping levels.

In the spectrum of the $n_{\text{corr}} = 1.14 \times 10^{19} \text{ cm}^{-3}$ epilayer, the coupled mode spectrum consists of two features: a relatively intense, broad mode near the TO phonon mode wavenumber (see Fig. 1) and a weaker, broader mode in the $\approx 250 \text{ cm}^{-1}$ to 500 cm^{-1} range (see Fig. 2). These features are attributed to high and low frequency coupled modes originating in the bulk.²⁸ A feature is also observed in the spectrum near the LO phonon mode wavenumber. This feature is attributed to scattering from the hole-depleted and/or hole-enriched region of the accumulation layer. Although the signal-to-noise ratio of this spectrum is relatively poor, this feature is broad and could be composed of at least two peaks: one with a wavenumber near that of the uid-GaSb LO mode wavenumber and one with a wavenumber lower than the uid-GaSb LO mode wavenumber. A peak at the uid-GaSb LO mode wavenumber would be attributed to scattering

from the hole-depleted region of the accumulation layer. A peak with a lower wavenumber than the uid-GaSb LO mode wavenumber would be consistent with scattering from a coupled mode in the hole-enriched region of the accumulation layer.²⁵⁻²⁷ Presumably, this feature is present in the spectra of the other epilayers, although a weak shoulder is observed at this wavenumber in the $n_{\text{corr}} = 2.05 \times 10^{18} \text{ cm}^{-3}$ epilayer spectrum, but is not resolved because of the similarity between the bulk and accumulation layer coupled mode wavenumbers.

The consistency of the GaSb spectral trends with those of bulk p-type GaAs and GaSb coupled mode spectra and the large Raman probe depth at this excitation wavelength relative to the accumulation layer width, indicates that the observed scattering signal originates primarily in the bulk for all epilayers. Accumulation layer scattering is weakly observed in the spectra of the $n_{\text{corr}} = 2.05 \times 10^{18} \text{ cm}^{-3}$ and $n_{\text{corr}} = 1.14 \times 10^{19} \text{ cm}^{-3}$ epilayers for which bulk and accumulation layer coupled mode scattering is spectrally resolved and the accumulation layer width is relatively thin.²⁸

2. Spectral models

A number of spectral models have been developed to describe coupled phonon-plasmon mode spectra in various III-V materials.^{6,9,50} These spectral models involve some form of the dielectric function and can be generally classified into three categories depending on the expression used to model the electronic contribution to the dielectric function. The three different expressions utilize either a so-called Lindhard-Mermin model, a hydrodynamical model, or a Drude model for the electronic contribution to the dielectric function.^{6,9,50,51} The model selected to describe the electronic contribution to the dielectric function dictates to what degree different processes in the phonon-plasmon system are treated. Four important processes that are treated differently by the various models are Landau damping of the collective plasmon

mode, spatial dispersion of the plasmon mode, band nonparabolicity, and finite temperature effects. The Lindhard-Mermin model accounts for Landau damping of the collective plasmon mode, spatial dispersion of the plasmon mode, band nonparabolicity, and finite temperature effects (and other electron-electron interactions).^{7-9,50,52,53} This model requires a relatively detailed understanding of the electronic band structure, typically including the band structure dependence on dopant concentration (e.g., band gap renormalization). The hydrodynamical model can be constructed so as to account for spatial dispersion of the plasmon mode, band nonparabolicity, and finite temperature effects but not Landau damping.^{7,50,51} Plasmon spatial dispersion is accounted for by introduction of a term composed of the root mean square velocity times the square of the scattering wavevector. Evaluation of this term requires knowledge of the effective mass in all relevant bands and potentially the carrier dependent effective mass in each band. This term is often approximated by assuming either classical or degenerate carrier statistics. By expressing this term using Fermi-Dirac integrals of order 1/2 and 3/2, this term can be made to apply in both classical and degenerate limits.^{7,50} However, a Fermi energy must be determined to solve these integrals. Accurate determination of the Fermi energy requires an understanding of band density of states as a function of dopant concentration.³⁵ To account for band nonparabolicity, a carrier dependent effective mass is typically utilized. Hence, the dependence of an optical effective mass on hole concentration must be known. The inclusion of finite temperature effects also requires solution of Fermi-Dirac integrals of order 1/2 and 3/2 and, consequently, determination of the Fermi energy. The Drude model ignores Landau damping, spatial dispersion of the plasmon, band nonparabolicity, and finite temperature effects.^{7,50,54} Despite the limitations of the Drude model, this model has the advantage that it requires the

fewest input parameters and is computationally inexpensive, particularly compared to the Lindhard-Mermin model.

Since the experimental coupled mode spectra yield only peak wavenumber and linewidth, limiting the unknown parameters in a spectral model to only two values improves confidence in the fitting procedure. The two parameters are typically hole concentration and a hole damping parameter. Hence, all other materials parameters must be well known or fit accuracy can be degraded. Unfortunately, utilization of the more sophisticated spectral models generally requires knowledge of materials parameters that are not well characterized for GaSb. If the heavy hole and light hole concentrations were known to a high degree of accuracy, the relevant properties could be potentially used as fit parameters. However, as discussed above, the accuracy of higher-level methods of calculating hole concentrations in GaSb is unknown. Hence, although it has been shown that Landau damping, spatial dispersion of the plasmon, band nonparabolicity, and finite temperature effects are important in n-InP,^{7,50} n⁺-GaAs,⁹ and n-InGaAs,⁸ and these effects are ignored in the Drude model, the Drude model was employed in this work. This was justified because it was deemed impossible, within the scope of this project, to evaluate the relative accuracy of different spectral models for determining hole concentration.

In this work, the coupled phonon-plasmon mode spectrum was simulated using a lineshape function to describe deformation-potential and electro-optic scattering mechanism:⁶

$$L_A(\omega) = \left(1 - e^{-\hbar\omega/k_B T}\right)^{-1} \left(\frac{\omega_0^2 - \omega^2}{\omega_{TO}^2 - \omega^2}\right)^2 \text{Im}\left\{\frac{-1}{\epsilon(\omega)}\right\} \quad (6)$$

where ω is the scattering frequency, \hbar ($= h/2\pi$) is the Planck constant, k_B is the Boltzmann constant, T is the thermodynamic temperature, ω_{TO} is the TO phonon frequency, $\epsilon(\omega)$ is the ω -dependent dielectric function, and ω_0 is defined as

$$\omega_0^2 = \omega_{\text{TO}}^2(1 + C) \quad (7)$$

where C is the (dimensionless) Faust-Henry coefficient. For coupled phonon-hole plasmon systems, $\varepsilon(\omega)$ can be described by⁵⁵

$$\varepsilon(\omega) = \varepsilon_\infty + \chi_{\text{ph}}(\omega) + \chi_{\text{intra}}(\omega) + \chi_{\text{inter}}(\omega) \quad (8)$$

where ε_∞ is the high frequency dielectric constant, $\chi_{\text{ph}}(\omega)$ is the phonon contribution to the dielectric function, $\chi_{\text{intra}}(\omega)$ is the contribution to the dielectric function from intra-valence band transitions, and $\chi_{\text{inter}}(\omega)$ is the contribution from inter-valence band transitions. In this model, $\chi_{\text{intra}}(\omega)$ and $\chi_{\text{inter}}(\omega)$ together make up the electronic contribution to the dielectric function. For a binary semiconductor, $\chi_{\text{ph}}(\omega)$ can be described by⁹

$$\chi_{\text{ph}}(\omega) = \varepsilon_\infty \frac{\omega_{\text{LO}}^2 - \omega_{\text{TO}}^2}{\omega_{\text{TO}}^2 - \omega^2 - i\gamma_{\text{ph}}\omega} \quad (9)$$

where ω_{LO} is the LO phonon frequency and γ_{ph} is the phonon damping parameter. $\chi_{\text{intra}}(\omega)$ is composed of contributions from the light and heavy hole intra-valence band transitions and can be expressed as:⁵⁵

$$\chi_{\text{intra}}(\omega) = -\varepsilon_\infty \left[\frac{(\omega_{\text{p}}^{\text{lh}})^2}{\omega^2 + i\gamma_{\text{p}}^{\text{lh}}\omega} + \frac{(\omega_{\text{p}}^{\text{hh}})^2}{\omega^2 + i\gamma_{\text{p}}^{\text{hh}}\omega} \right] \quad (10)$$

where $\gamma_{\text{p}}^{\text{i}}$ is the respective hole plasmon damping parameter and $\omega_{\text{p}}^{\text{i}}$ is the respective hole plasma frequency. Equation (10) can be simplified by employing an average hole optical effective mass, m_{opt}^* , given by⁵⁶

$$\frac{1}{m_{\text{opt}}^*} = \frac{m_{\text{lh}}^{1/2} + m_{\text{hh}}^{1/2}}{m_{\text{lh}}^{3/2} + m_{\text{hh}}^{3/2}} \quad (11)$$

Using Eq. (11), Eq. (10) can be simplified to

$$\chi_{\text{intra}}(\omega) = -\varepsilon_{\infty} \left(\frac{\omega_{\text{P}}^2}{\omega^2 + i\gamma_{\text{P}}\omega} \right) \quad (12)$$

where γ_{P} is the effective hole damping parameter and ω_{P} is the effective hole plasma frequency and is given by

$$\omega_{\text{P}} = \left(\frac{n_{\text{RS}} e^2}{\varepsilon_{\infty} \varepsilon_0 m_{\text{opt}}^*} \right)^{1/2} \quad (13)$$

where n_{RS} is the total hole concentration (optically-determined), e is the elementary charge, and ε_0 is the electric constant.

3. Hole concentration determination from Raman spectra

To quantitatively determine the hole concentration from the Raman spectra in this work, a global search minimization was performed to minimize the sum of the residuals squared between an experimental Raman spectrum and a simulated Raman spectrum. The only two fit parameters in this model are contained in $\chi_{\text{intra}}(\omega)$: the total hole concentration (n_{RS}) and the effective plasmon damping parameter (γ_{P}). Experimental spectra include contributions from bulk coupled mode scattering as well as relatively weak scattering from the TO phonon mode, second order phonon modes, and the surface accumulation layer. Contributions from these four scattering sources were included in the simulated Raman spectra. The bulk coupled mode scattering contribution to a simulated spectrum was calculated using Eq. (6) with $\chi_{\text{ph}}(\omega)$ and $\chi_{\text{intra}}(\omega)$ being described by Eq. (9) and Eq. (12), respectively. Because these measurements were performed at room temperature, it was assumed that $\chi_{\text{inter}}(\omega)$ was negligible.⁵⁷ Respective scattering signal due to the TO phonon mode, second order phonon modes, and the surface accumulation layer was assumed to be identical for all spectra. The peak parameters from the TO phonon mode and

second order feature at 273 cm^{-1} were obtained from the uid-GaSb spectrum. During a fit, the amplitude of each of these features was held constant and the peak wavenumber was allowed to vary within relatively narrow constraints (to compensate for instrumental effects). The TO phonon and second order mode wavenumber were allowed to vary between 225.5 cm^{-1} to 226.6 cm^{-1} and 270 cm^{-1} to 273 cm^{-1} , respectively. The peak parameters from the accumulation layer scattering was obtained from a fit to the $\approx 235 \text{ cm}^{-1}$ feature in the $n_{\text{corr}} = 1.14 \times 10^{19} \text{ cm}^{-3}$ epilayer spectrum (the accumulation layer-related scattering signal).²⁸ Although accumulation layer-related scattering signal could not be resolved from bulk coupled mode scattering in all spectra, it was assumed that the accumulation layer-related scattering signal in the $n_{\text{corr}} = 1.14 \times 10^{19} \text{ cm}^{-3}$ epilayer spectrum was representative. During a fit, the amplitude of the accumulation layer-related feature was held constant and the peak wavenumber was allowed to vary between 234 cm^{-1} to 235.5 cm^{-1} (based on the magnitude of the shifts observed in 488 nm excitation spectra²⁸ and the instrumental bandpass). The parameter values used in these simulations are listed in Table III (see also Table I for effective mass values).

The assumption that the accumulation layer-related scattering signal in the $n_{\text{corr}} = 1.14 \times 10^{19} \text{ cm}^{-3}$ epilayer spectrum was representative of all accumulation layer scattering was made for simplicity and, although not strictly true, is not expected to introduce significant error. This expectation was justified as follows. Accumulation layer-related signal can be resolved to some degree only in the $n_{\text{corr}} = 2.05 \times 10^{18} \text{ cm}^{-3}$ and the $n_{\text{corr}} = 1.14 \times 10^{19} \text{ cm}^{-3}$ epilayer spectra. In the $n_{\text{corr}} = 1.14 \times 10^{19} \text{ cm}^{-3}$ epilayer spectrum the accumulation layer-related scattering is observed as a reasonably well-resolved feature at $\approx 235 \text{ cm}^{-1}$. In the $n_{\text{corr}} = 2.05 \times 10^{18} \text{ cm}^{-3}$ epilayer spectrum the accumulation layer-related scattering is observed as a weak shoulder at $\approx 235.6 \text{ cm}^{-1}$. The accumulation layer-related scattering feature area is approximately 9% and 2%

of the area of the respective bulk coupled mode peak in the $n_{\text{corr}} = 2.05 \times 10^{18} \text{ cm}^{-3}$ and $1.14 \times 10^{19} \text{ cm}^{-3}$ epilayer spectra, respectively. To determine if the relative contribution of the accumulation layer scattering in the $n_{\text{corr}} = 3.45 \times 10^{17} \text{ cm}^{-3}$ and $9.89 \times 10^{17} \text{ cm}^{-3}$ epilayer spectra is comparable to that in the $n_{\text{corr}} = 2.05 \times 10^{18} \text{ cm}^{-3}$ and $1.14 \times 10^{19} \text{ cm}^{-3}$ epilayer spectra, relative peak intensities of the bulk coupled modes and accumulation layer-related modes were compared. The bulk coupled mode scattering intensity in the $n_{\text{corr}} = 3.45 \times 10^{17} \text{ cm}^{-3}$, $9.89 \times 10^{17} \text{ cm}^{-3}$, and $2.05 \times 10^{18} \text{ cm}^{-3}$ epilayer spectra relative to that in the $n_{\text{corr}} = 1.14 \times 10^{19} \text{ cm}^{-3}$ epilayer spectrum is approximately 7.4, 3.2, and 1.7, respectively (see Fig. 1). The accumulation layer-related scattering intensity ratios were determined from Raman spectra excited with 488 nm radiation. Figure 3 shows the spectra of the intentionally doped p-type GaSb epilayers compared to the uid-GaSb spectrum excited with 488 nm radiation. The vertical line indicates the wavenumber of the LO phonon mode in the uid-GaSb spectrum. The Raman probe depth with 488 nm excitation is on the order of ≈ 10 nm or less and, hence, accumulation layer-related scattering dominates the scattering signal observed in these spectra (although some bulk coupled mode scattering is observed at higher hole concentrations).²⁸ The accumulation layer-related scattering intensity in the $n_{\text{corr}} = 3.45 \times 10^{17} \text{ cm}^{-3}$, $9.89 \times 10^{17} \text{ cm}^{-3}$, and $2.05 \times 10^{18} \text{ cm}^{-3}$ epilayer spectra relative to that in the $n_{\text{corr}} = 1.14 \times 10^{19} \text{ cm}^{-3}$ epilayer spectrum is approximately 2.3, 1.7, and 1.7, respectively (see Fig. 3). Since neither 488 nm and 752.55 nm radiation is near an electronic resonance,⁵⁹ it is assumed that the relative scattering cross sections are nominally identical for the series of spectra obtained with 488 nm and the series obtained with 752.55 nm excitation. Both the bulk coupled mode and accumulation layer-related scattering intensities decrease with increasing hole concentration. However, the accumulation layer-related scattering intensity decreases at a faster rate than the bulk coupled mode intensity.

Therefore, it is estimated that the relative contribution of the accumulation layer-related signal in the $n_{\text{corr}} = 3.45 \times 10^{17} \text{ cm}^{-3}$ and $9.89 \times 10^{17} \text{ cm}^{-3}$ epilayer spectra is smaller than the relative contribution observed in the $n_{\text{corr}} = 2.05 \times 10^{18} \text{ cm}^{-3}$ and $1.14 \times 10^{19} \text{ cm}^{-3}$ epilayer spectra.

Figures 4, 5, 6, and 7 shown the truncated experimental Raman spectrum (dots) and associated best-fit simulated spectrum (solid line) for the $n_{\text{corr}} = 3.45 \times 10^{17} \text{ cm}^{-3}$, $9.89 \times 10^{17} \text{ cm}^{-3}$, $2.05 \times 10^{18} \text{ cm}^{-3}$, and $1.14 \times 10^{19} \text{ cm}^{-3}$ epilayers, respectively. Even though a relatively simple spectral model is employed, the fits are reasonable for all spectra, especially for the epilayers with lower doping levels. The DMZn mole fraction in the reactor during deposition and the corresponding n_{corr} value and Raman spectroscopically-determined hole concentration, n_{RS} , and effective plasmon damping parameter, γ_{P} , are listed in Table IV.

C. Comparison of Raman spectroscopic and Hall effect measurement results

The percent differences between the n_{RS} and n_{corr} values $[(n_{\text{RS}} - n_{\text{corr}})/n_{\text{corr}} \times 100]$ are plotted as a function of n_{corr} in Fig. 8. Although only a limited number of epilayers were investigated, it appears from Fig 8 that this spectral models produces n_{RS} values that are higher than n_{corr} at hole concentrations lower than $\approx 7.5 \times 10^{17} \text{ cm}^{-3}$ and n_{RS} values that are lower than n_{corr} at low hole concentrations higher than $\approx 7.5 \times 10^{17} \text{ cm}^{-3}$. These trends are attributed in part to the limitations of the Drude form of the electronic contribution to the dielectric function.^{7,50} At low carrier concentrations in n-InP, a Drude model overestimates carrier concentration because plasmon spatial dispersion is ignored. At high carrier concentrations in n-InP, a Drude model underestimates carrier concentration because band nonparabolicity is ignored.^{7,50} Although the material systems are different, these effects probably still contribute to the differences between Hall effect and Raman spectroscopic measurement of hole concentration. In addition, at high hole concentrations, the neglect of inter-valence band scattering may

contribute,²¹ as may the assumption of a single carrier type with an average effective mass [see Eq. (11)]. Also, neglect of Landau damping may be a factor in the difference between the hole concentration obtained with the different techniques. Based on the magnitudes of the hole effective masses (see Table I), it is expected that the low-effective mass light holes may be Landau damped at higher hole concentrations, while the heavy holes probably are not Landau damped.⁸ However, since the concentration of light holes is only ≈ 0.08 times that of the heavy holes [see Eq. (3)], neglect of Landau damping may not be a large source of error at any hole concentrations. Uncertainties in the GaSb materials parameters also contribute to the deviations between the hole concentration values. The fit results depended strongly on effective mass values. For example, if values of 0.48 and 0.41 are employed for the heavy hole and light hole effective mass,³³ respectively, n_{RS} values are increased by about 80% relative to the values obtained using the effective masses listed in Table I. However, given the relatively simple model employed here and the issues associated with such a model, the agreement between the n_{RS} and n_{corr} is reasonable.

IV. CONCLUSIONS

Room temperature p-GaSb bulk coupled mode spectra were measured as a function of hole concentration. These spectra were obtained using an optical system based on 752.55 nm excitation in order to obtain more sensitivity to bulk GaSb coupled mode scattering than possible with visible wavelength excitation-based systems. A relatively simple Drude model for the electronic contribution to the dielectric function was evaluated for determination of hole concentration from the bulk coupled mode spectra. Although this model is known to possess limitations, the use of this model was justified because it was deemed impossible, within the scope of this project, to evaluate the relative accuracy of more sophisticated spectral models for

determining hole concentration. Optically-derived values for hole concentration were determined by minimizing the sum of the residuals squared between an experimental and simulated spectrum as a function of total hole concentration and plasmon damping parameter. Hole concentrations obtained from the Raman spectroscopic measurements deviated from the values determined from single field Hall effect measurements that were corrected to account for two band conduction by $\approx 20\%$ to $\approx 65\%$. These deviations were attributed to the limitations of the spectral model employed and uncertainties in GaSb materials properties.

ACKNOWLEDGMENTS

The authors gratefully acknowledge D. A. Shiau for assistance in the growth of epilayers and in the performance of the single magnetic field Hall effect measurements, M. Muñoz for GaSb spectroscopic ellipsometric data, and H. S. Bennett for helpful discussions.

REFERENCES

- ¹A. Aardvark, N. J. Mason, and P. J. Walker, *Prog. Cryst. Growth Characterization Mater.* **35**, 207-241 (1997).
- ²R. M. Biefeld, *Mater. Sci. Eng., R* **36**, 105-142 (2002).
- ³P. S. Dutta, H. L. Bhat, and V. Kumar, *J. Appl. Phys.* **81**, 5821-5870 (1997).
- ⁴B. C. Dodrill, J. R. Lindemuth, B. J. Kelley, G. Du, and J. R. Meyer, *Compound Semicond.* **7**, 58-60 (2001).
- ⁵H. Ehsani, I. Bhat, C. Hitchcock, R. J. Gutmann, G. Charache, and M. Freeman, *J. Cryst. Growth* **195**, 385-390 (1998).
- ⁶G. Abstreiter, M. Cardona, and A. Pinczuk, in *Topics in Applied Physics; Vol. 54* (1984), p. 5-150.
- ⁷L. Artus, R. Cusco, J. Ibanez, N. Blanco, and G. Gonzalez-Diaz, *Phys. Rev. B* **60**, 5456-5463 (1999).
- ⁸R. Cusco, L. Artus, S. Hernandez, J. Ibanez, and M. Hopkinson, *Phys. Rev. B* **65**, 0352101-0352107 (2001).
- ⁹M. Ramsteiner, J. Wagner, P. Hiesinger, K. Kohler, and U. Rossler, *J. Appl. Phys.* **73**, 5023-5026 (1993).
- ¹⁰R. Fukasawa, S. Katayama, A. Hasegawa, and K. Ohta, *J. Phys. Soc. Jpn.* **57**, 3632-3640 (1988).
- ¹¹R. Fukasawa and S. Perkowitz, *Phys. Rev. B* **50**, 14119-14124 (1994).
- ¹²R. Fukasawa and S. Perkowitz, *Jpn. J. Appl. Phys., Part 1* **35**, 132-133 (1996).
- ¹³R. Fukasawa, M. Wakaki, K. Ohta, and H. Okumura, *Jpn. J. Appl. Phys., Part 1* **25**, 652-653 (1986).

- ¹⁴M. Gargouri, B. Prevot, and C. Schwab, *J. Appl. Phys.* **62**, 3902-3911 (1987).
- ¹⁵G. Irmer, M. Wenzel, and J. Monecke, *Phys. Rev. B* **56**, 9524-9538 (1997).
- ¹⁶T. Kamijoh, A. Hashimoto, H. Takano, and M. Sakuta, *J. Appl. Phys.* **59**, 2382-2386 (1986).
- ¹⁷A. Mlayah, R. Carles, G. Landa, E. Bedel, and A. Munozyague, *J. Appl. Phys.* **69**, 4064-4070 (1991).
- ¹⁸D. Olego and M. Cardona, *Solid State Commun.* **32**, 375-378 (1979).
- ¹⁹D. Olego and M. Cardona, *Phys. Rev. B* **24**, 7217-7232 (1981).
- ²⁰M. Seon, M. Holtz, W. M. Duncan, and T. S. Kim, *J. Appl. Phys.* **85**, 7224-7230 (1999).
- ²¹K. Wan and J. F. Young, *Phys. Rev. B* **41**, 10772-10779 (1990).
- ²²K. Wan, J. F. Young, R. L. S. Devine, W. T. Moore, A. J. Springthorpe, C. J. Miner, and P. Mandeville, *J. Appl. Phys.* **63**, 5598-5600 (1988).
- ²³T. Yuasa and M. Ishii, *Phys. Rev. B* **35**, 3962-3970 (1987).
- ²⁴X. K. Chen, R. Wiersma, C. X. Wang, O. J. Pitts, C. Dale, C. R. Bolognesi, and S. P. Watkins, *Appl. Phys. Lett.* **80**, 1942-1944 (2002).
- ²⁵R. Dornhaus, R. L. Farrow, and R. K. Chang, *Solid State Commun.* **35**, 123-126 (1980).
- ²⁶R. Dornhaus, R. L. Farrow, R. K. Chang, and R. M. Martin, in *Light Scattering in Solids*, edited by J. L. Birman, H. Z. Cummins, and K. K. Rebane (Plenum Press, New York, 1979), p. 299-305.
- ²⁷R. L. Farrow, R. K. Chang, and R. M. Martin; *Vol. Physics of Semiconductors, Conference Series Vol. 43*, edited by B. L. H. Wilson (Institute of Physics, Edinburgh, 1979), p. 485-488.
- ²⁸J. E. Maslar, W. S. Hurst, and C. A. Wang "Raman Spectroscopy of n-Type and p-Type GaSb with Multiple Excitation Wavelengths," *Appl. Spectrosc.*, submitted (2006).
- ²⁹C. A. Wang, *J. Cryst. Growth* **191**, 631-640 (1998).

- ³⁰C. A. Wang, D. A. Shiau, R. K. Huang, C. T. Harris, and M. K. Connors, *J. Cryst. Growth* **261**, 379-384 (2004).
- ³¹M. W. Heller and R. G. Hamerly, *J. Appl. Phys.* **57**, 4626-4632 (1985).
- ³²P. C. Mathur and S. Jain, *Phys. Rev. B* **19**, 3152-3158 (1979).
- ³³I. M. J. R. R.-M. L. R. Vurgaftman, *J. Appl. Phys.* **89**, 5815-5875 (2001).
- ³⁴H. S. Bennett, H. Hung, and A. Heckert, *J. Appl. Phys.* **98** (2005).
- ³⁵H. S. Bennett and J. R. Lowney, *J. Appl. Phys.* **62**, 521-527 (1987).
- ³⁶J. S. Blakemore, *J. Appl. Phys.* **53**, R123-R181 (1982).
- ³⁷A. Raymond, J. L. Robert, and C. Bernard, *J. Phys. C: Solid State Phys.* **12**, 2289-2293 (1979).
- ³⁸P. Van Halen, *J. Appl. Phys.* **59**, 2264-2265 (1986).
- ³⁹P. Van Halen and D. L. Pulfrey, *J. Appl. Phys.* **57**, 5271-5274 (1985).
- ⁴⁰D. Barjon, A. Raymond, B. Pistoulet, and J. L. Robert, *J. Phys. Chem. Solids* **34**, 2231-2234 (1973).
- ⁴¹J. L. Robert, B. Pistoulet, D. Barjon, and A. Raymond, *J. Phys. Chem. Solids* **34**, 2221-2230 (1973).
- ⁴²J. P. Nerou, A. Filion, and P. E. Girard, *J. Phys. C: Solid State Phys.* **9**, 479-489 (1976).
- ⁴³G. R. Bell, C. F. McConville, and T. S. Jones, *Phys. Rev. B* **54**, 2654-2661 (1996).
- ⁴⁴W. Mönch, in *Semiconductor Surfaces and Interfaces* (Springer-Verlag, Berlin, 1993), p. 19-29.
- ⁴⁵W. Kauschke, N. Mestres, and M. Cardona, *Phys. Rev. B* **36**, 7469-7485 (1987).
- ⁴⁶R. Trommer and A. K. Ramdas, in *Physics of Semiconductors, 1978; Vol. 43*, edited by B. L. H. Wilson (Institute of Physics, Edinburgh, 1979), p. 585-588.
- ⁴⁷T. Sekine, K. Uchinokura, and E. Matsuura, *Solid State Commun.* **18**, 1337-1340 (1976).

- ⁴⁸P. B. Klein and R. K. Chang, Phys. Rev. B **14**, 2498-2502 (1976).
- ⁴⁹G. Abstreiter, E. Bauser, A. Fischer, and K. Ploog, Appl. Phys. **16**, 345-352 (1978).
- ⁵⁰J. Ibanez, R. Cusco, and L. Artus, Phys. Status Solidi B **223**, 715-722 (2001).
- ⁵¹U. Nowak, W. Richter, and G. Sachs, Phys. Status Solidi B **108**, 131-143 (1981).
- ⁵²S. Ernst, A. R. Goni, K. Syassen, and M. Cardona, Phys. Rev. B **53**, 1287-1293 (1996).
- ⁵³W. Richter, U. Nowak, H. Jurgensen, and U. Rossler, Solid State Commun. **67**, 199-204 (1988).
- ⁵⁴B. Boudart, B. Prevot, and C. Schwab, Appl. Surf. Sci. **50**, 295-299 (1991).
- ⁵⁵G. Irmer, W. Siegel, G. Kuhnel, J. Monecke, F. M. M. Yasuoka, B. H. Bairamov, and V. V. Toporov, Semicond. Sci. Technol. **6**, 1072-1078 (1991).
- ⁵⁶O. Madelung, in *Physics of III-V Compounds* (John Wiley & Sons, Inc., New York, 1964), p. 42-103.
- ⁵⁷G. Irmer, J. Monecke, and M. Wenzel, J. Phys.: Condens. Matter **9**, 5371-5382 (1997).
- ⁵⁸A. Y. Vul', M. E. Levinshtein, S. L. Rumyantsev, and M. S. Shur, in *Handbook Series on Semiconductor Parameters: Vol. 1, Si, Ge, C (Diamond), GaAs, GaP, GaSb, InAs, InP, InSb* (World Scientific Publishing Co., Singapore, 1996), p. 125-146.
- ⁵⁹M. Munoz, K. Wei, F. H. Pollak, J. L. Freeouf, and G. W. Charache, Phys. Rev. B **60**, 8105-8110 (1999).

Table I. Parameter values used in the correction of the single field Hall effect measurement results to account for two-band conduction.

Parameter	Value
Light hole effective mass, m_{lh}	$0.050m_0^a$
Heavy hole effective mass, m_{hh}	$0.28m_0^a$
Hall scattering factor for light holes, r_{lh}	1.0^b
Hall scattering factor for heavy holes, r_{hh}	1.0^b
Anisotropy factor for light holes, K_{lh}	1.66^c
Anisotropy factor for heavy holes, K_{hh}	3.00^c
Shape factor for light holes, $F(K_{lh})$	0.98 (calculated)
Shape factor for heavy holes, $F(K_{hh})$	0.92 (calculated)
Ratio of heavy hole to light hole mobility, μ_{hh}/μ_{lh}	0.17^c

^aReference 31.

^bReference 40.

^cReference 41.

Table II. The DMZn mole fraction in the reactor during deposition of the epilayers investigated in this work and the corresponding the single magnetic field Hall effect measurement hole concentration, n_{Hall} , and mobility, μ_{Hall} , and corrected hole concentration, n_{corr} .

DMZn Mole Fraction	n_{Hall} (cm^{-3})	μ_{Hall} ($\text{cm}^2/\text{V-s}$)	n_{corr} (cm^{-3})
0	1.44×10^{16}	804	2.58×10^{16}
1×10^{-6}	1.92×10^{17}	677	3.45×10^{17}
2×10^{-6}	5.51×10^{17}	570	9.89×10^{17}
4×10^{-6}	1.14×10^{18}	477	2.05×10^{18}
10×10^{-6}	6.38×10^{18}	290	1.14×10^{19}

Table III. Parameter values used in the Raman spectral simulations (see also Table I for effective mass values).

Parameter	Value
High frequency dielectric constant, ϵ_∞	14.4 ^a
Faust-Henry coefficient, C	-0.23 ^b
TO phonon frequency, ω_{TO}	226 cm ^{-1c}
LO phonon frequency, ω_{LO}	236 cm ^{-1c}
Phonon damping parameter, γ_{ph}	0.001 ^c

^aReference 58.

^bReference 45.

^cThis work.

Table IV. The DMZn mole fraction in the reactor during deposition of the intentionally doped epilayers investigated in this work and the corresponding corrected hole concentration, n_{corr} , and Raman spectroscopically-determined hole concentration, n_{RS} , and effective plasmon damping parameter, γ_{P} .

DMZn Mole Fraction	n_{corr} (cm^{-3})	n_{RS} (cm^{-3})	γ_{P} (cm^{-1})
1×10^{-6}	3.45×10^{17}	5.63×10^{17}	448
2×10^{-6}	9.89×10^{17}	7.68×10^{17}	283
4×10^{-6}	2.05×10^{18}	1.23×10^{18}	240
10×10^{-6}	1.14×10^{19}	5.25×10^{18}	217

FIGURE CAPTIONS

Figure 1. The Raman spectra of the intentionally doped p-type GaSb epilayers compared to the uid-GaSb spectrum. The intensity of the most intense feature is normalized to unity in each spectrum and the spectra are offset on the intensity scale. The vertical line is shown as an aid to the eye and is located at 235.9 cm^{-1} .

Figure 2. The Raman spectra of the intentionally doped p-type GaSb epilayers compared to the uid-GaSb spectrum (instrumental bandpass $\approx 2.9 \text{ cm}^{-1}$). The spectra are offset on the intensity scale. The vertical line is shown as an aid to the eye and is located at 235.9 cm^{-1} .

Figure 3. The Raman spectra of the intentionally doped p-type GaSb epilayers compared to the uid-GaSb spectrum. All spectra were excited with 488 nm radiation. The spectra are offset on the intensity scale. The vertical line is shown as an aid to the eye and is located at 234.5 cm^{-1} .

Figure 4. The truncated experimental Raman spectrum (dots) and associated best-fit simulated spectrum (solid line) for the $n_{\text{corr}}=3.45 \times 10^{17} \text{ cm}^{-3}$ epilayer.

Figure 5. The truncated experimental Raman spectrum (dots) and associated best-fit simulated spectrum (solid line) for the $n_{\text{corr}}=9.89 \times 10^{17} \text{ cm}^{-3}$ epilayer.

Figure 6. The truncated experimental Raman spectrum (dots) and associated best-fit simulated spectrum (solid line) for the $n_{\text{corr}}=2.05 \times 10^{18} \text{ cm}^{-3}$ epilayer.

Figure 7. The truncated experimental Raman spectrum (dots) and associated best-fit simulated spectrum (solid line) for the $n_{\text{corr}}=1.14 \times 10^{19} \text{ cm}^{-3}$ epilayer.

Figure 8. The percent differences between the n_{RS} , and n_{corr} values $[(n_{\text{RS}} - n_{\text{corr}})/n_{\text{corr}} \times 100]$ plotted as a function of n_{corr} .

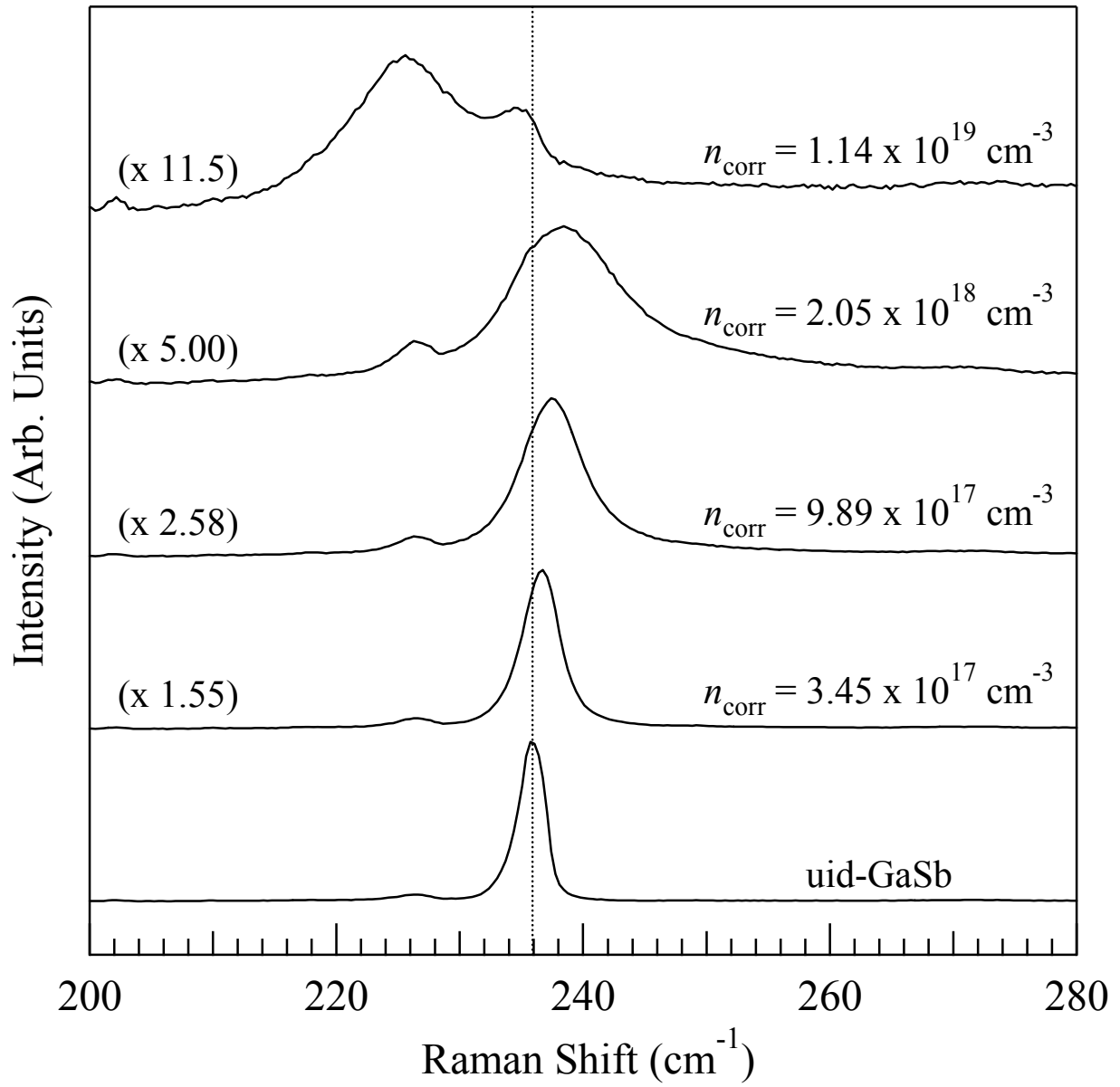


Figure 1

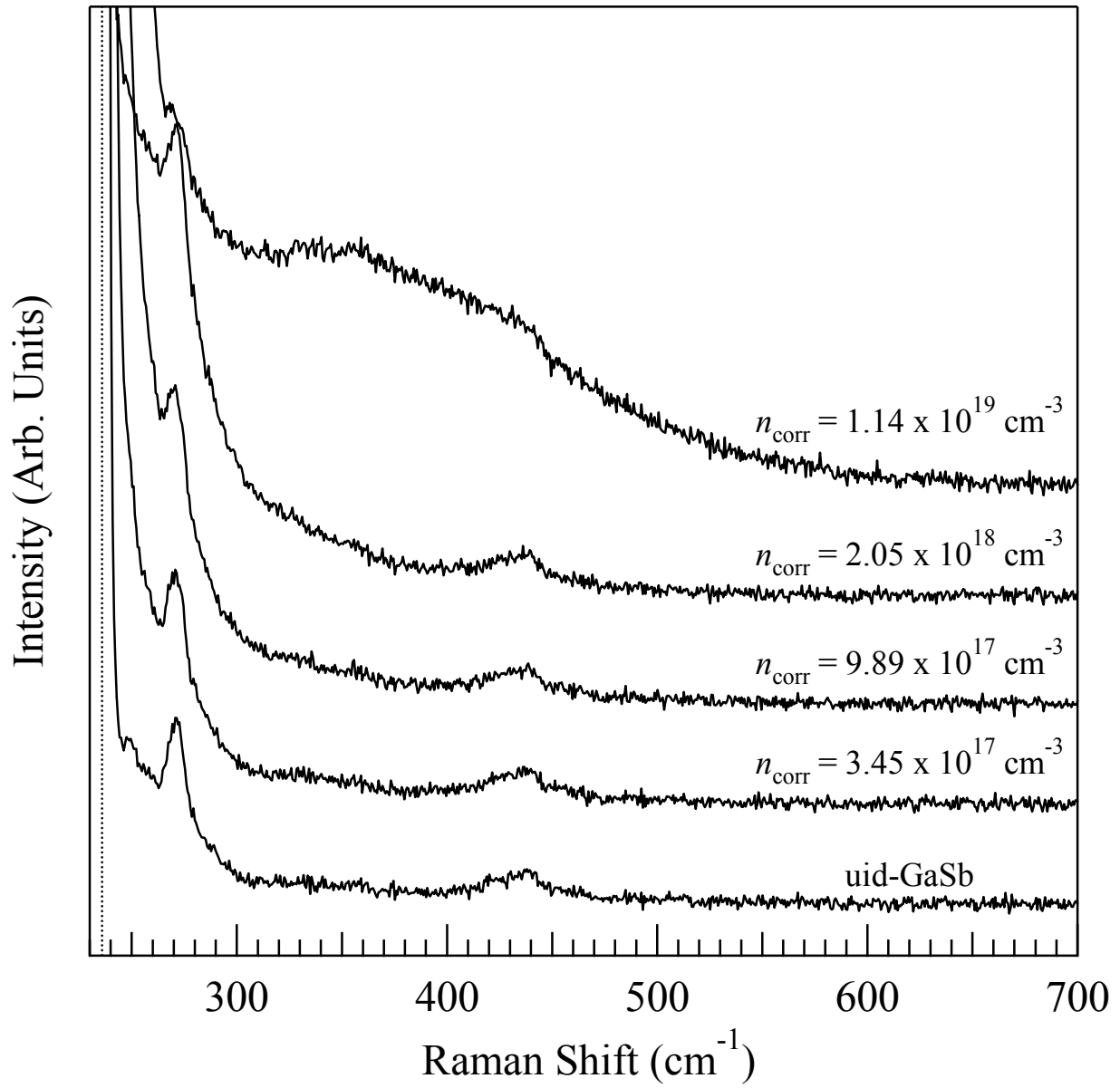


Figure 2

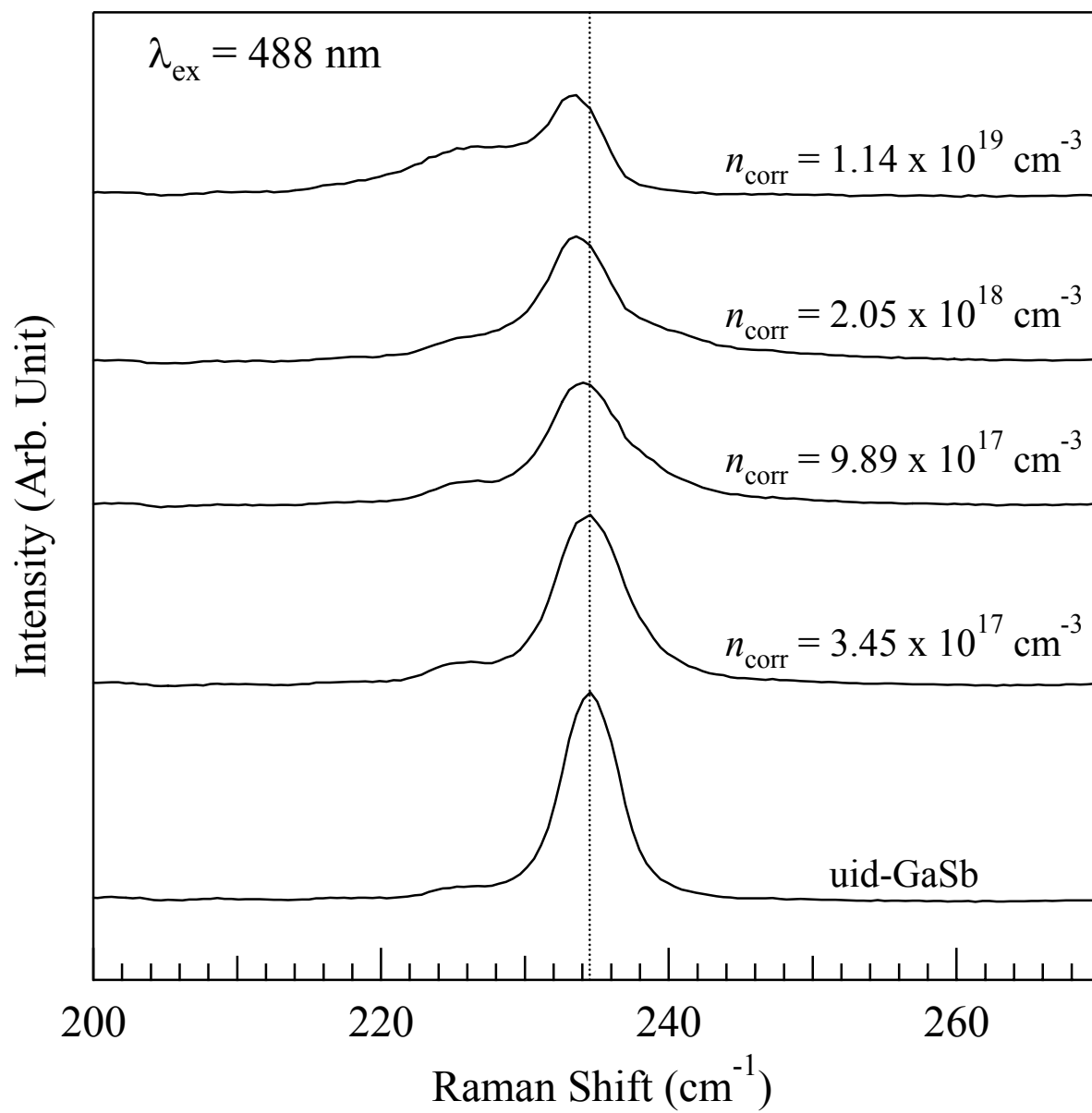


Figure 3

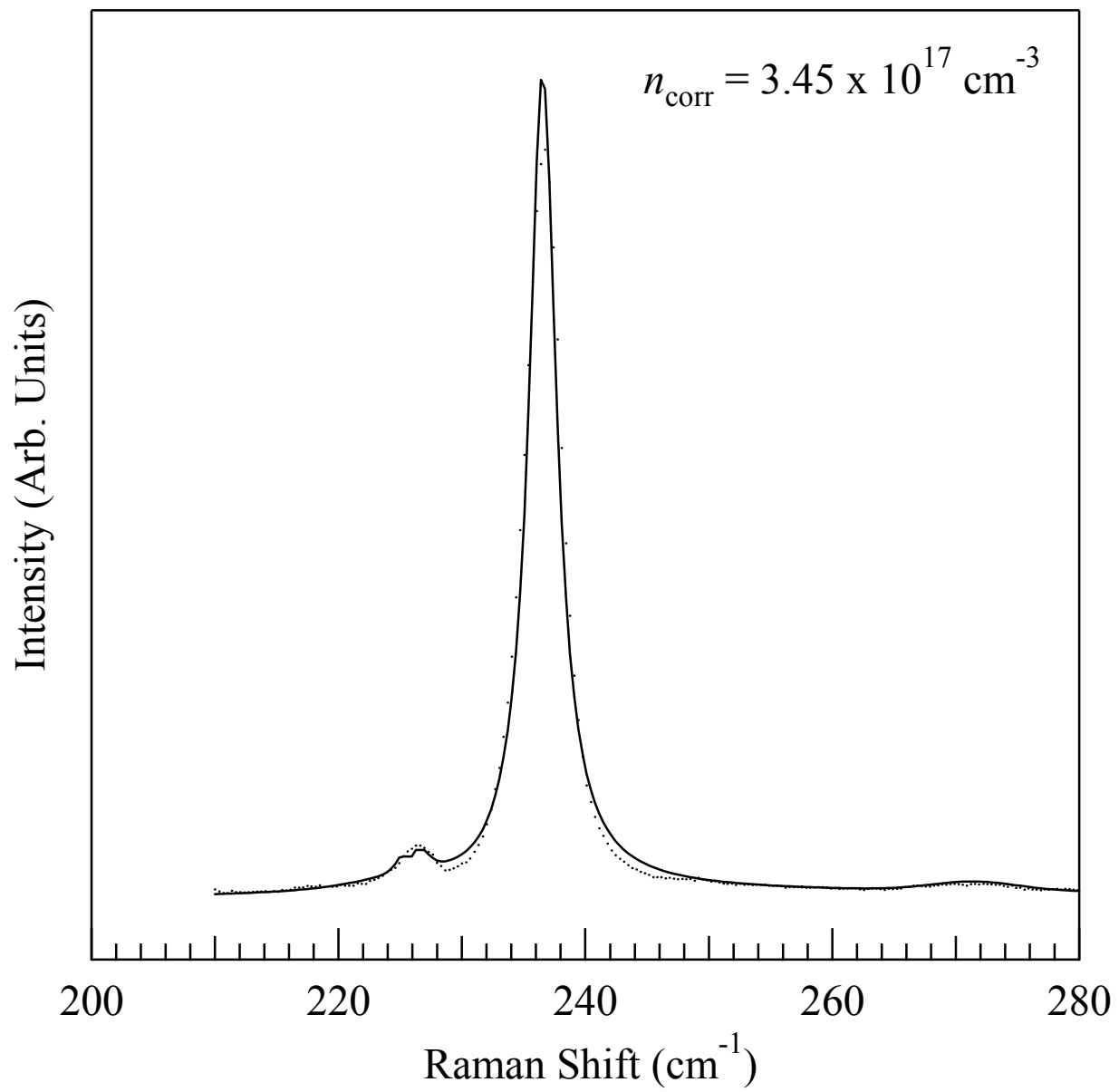


Figure 4

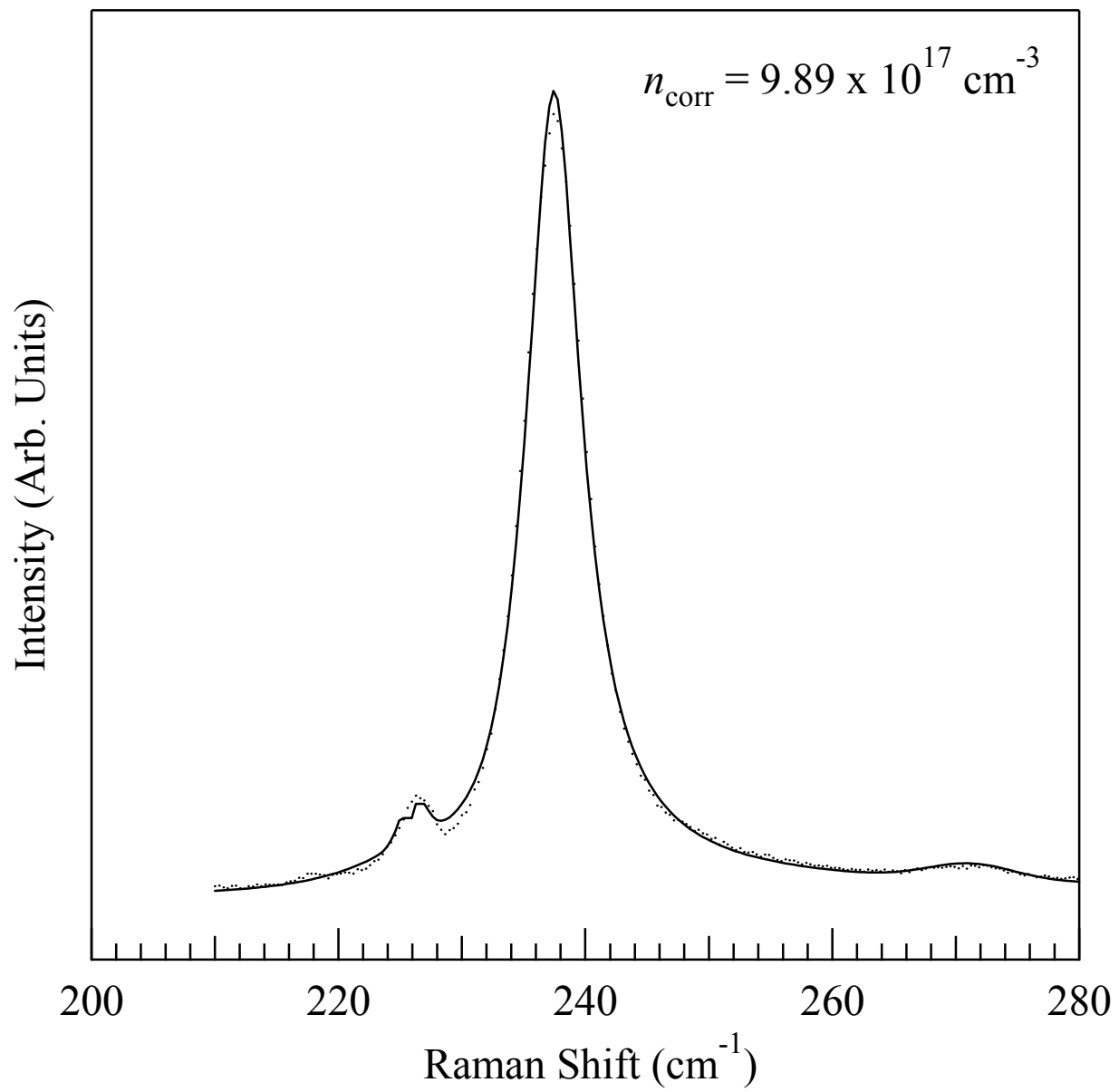


Figure 5

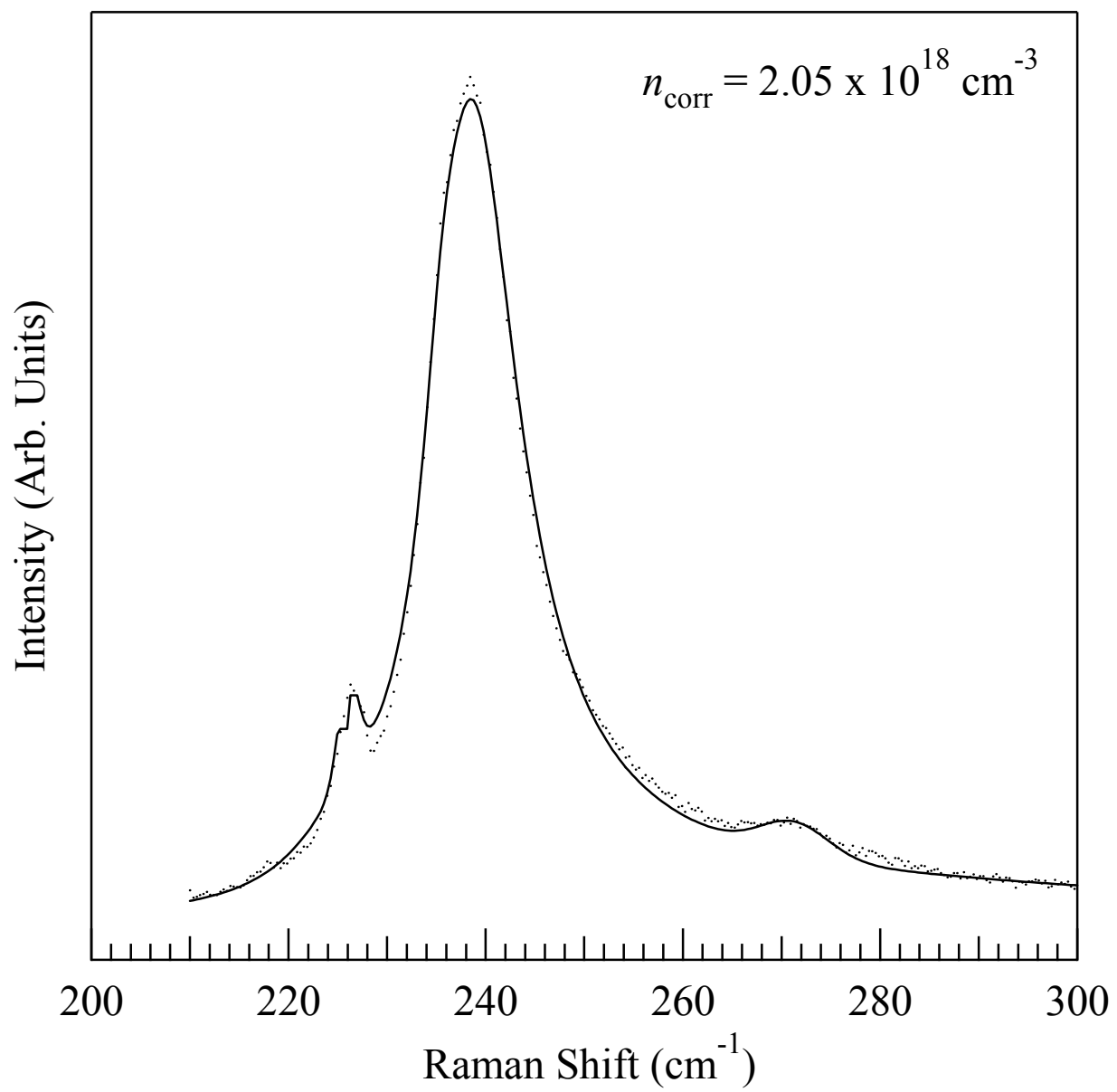


Figure 6

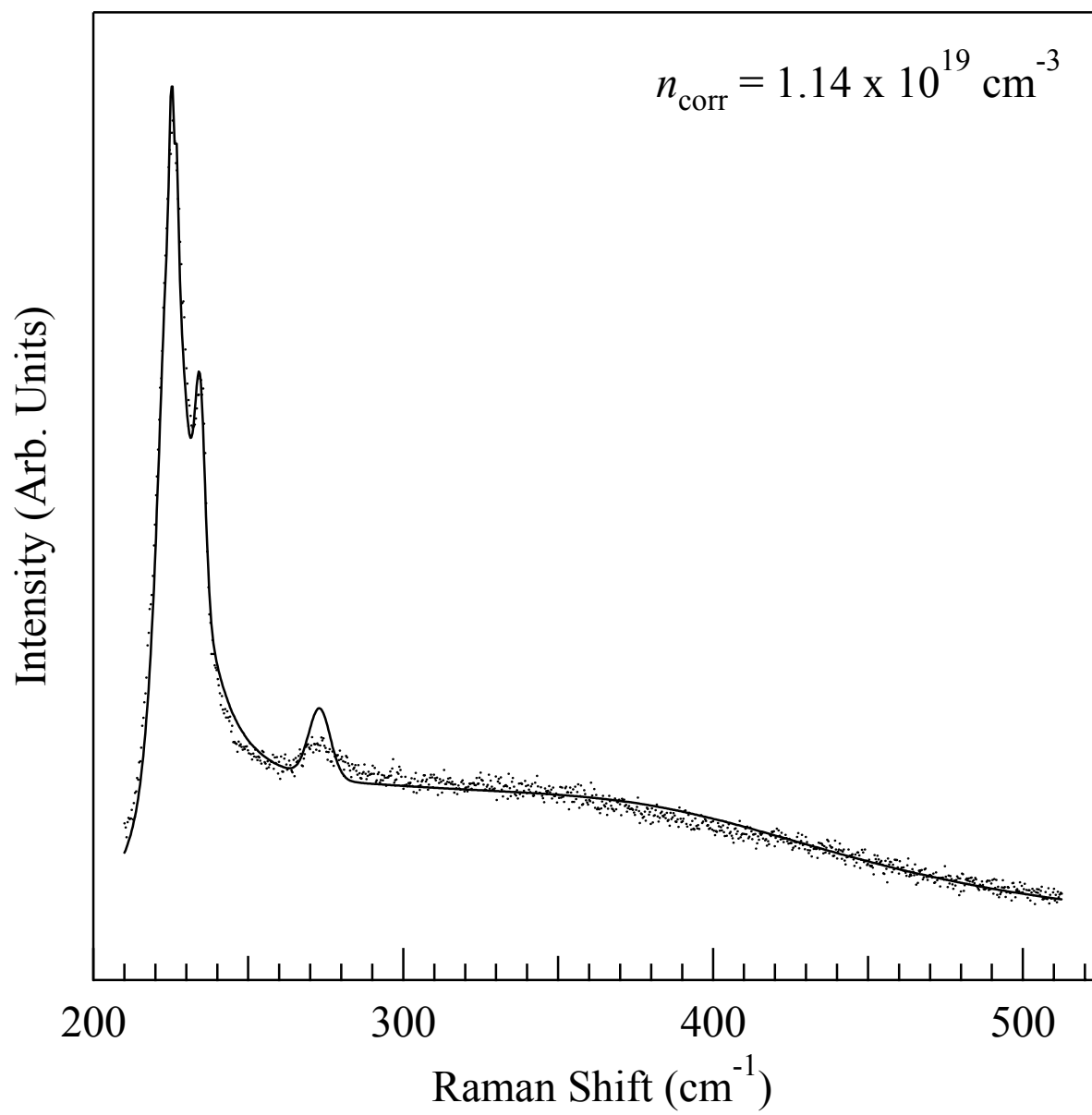


Figure 7

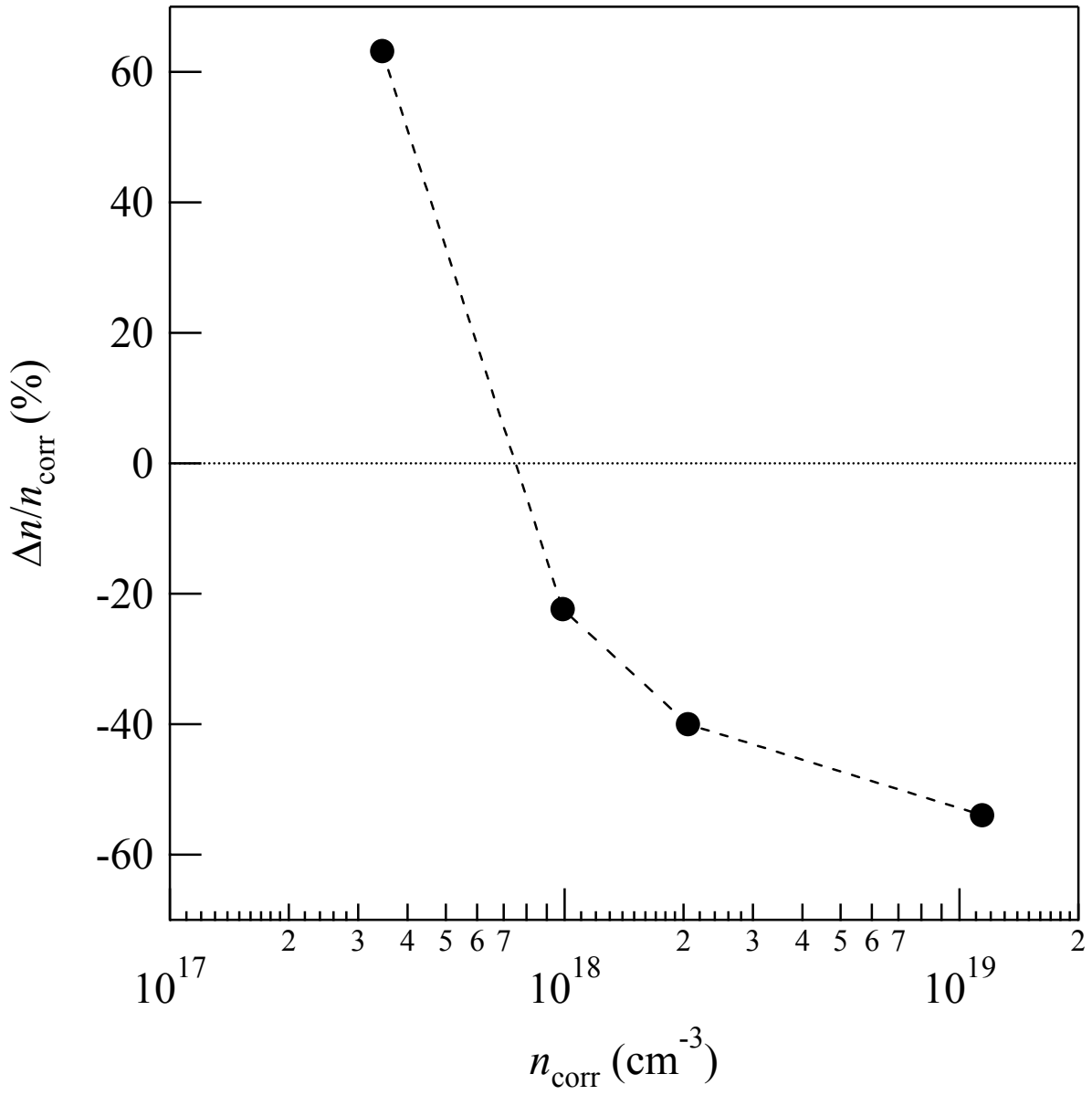


Figure 8